Comparison of Soil Moisture Retrieval Models using Polarimetric SAR data

Sahu, Uddesh[1] Rao, Y.S[1]; Bhogapurapu, Narayanarao[2]

[1]IIT Bombay, India; [2]University of Massachusetts, Amherst

Soil moisture/permittivity

Soil moisture: Amount of water stored in the unsaturated soil

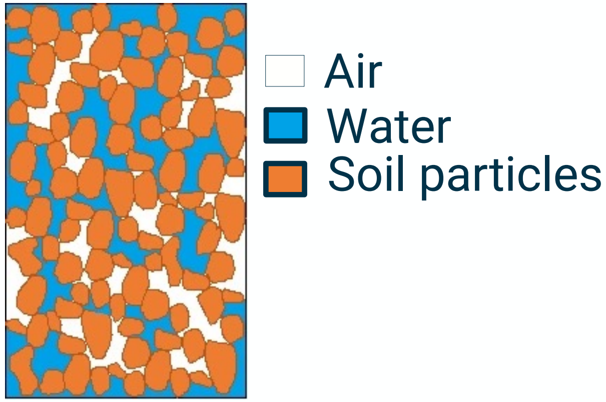

Cross-section soil

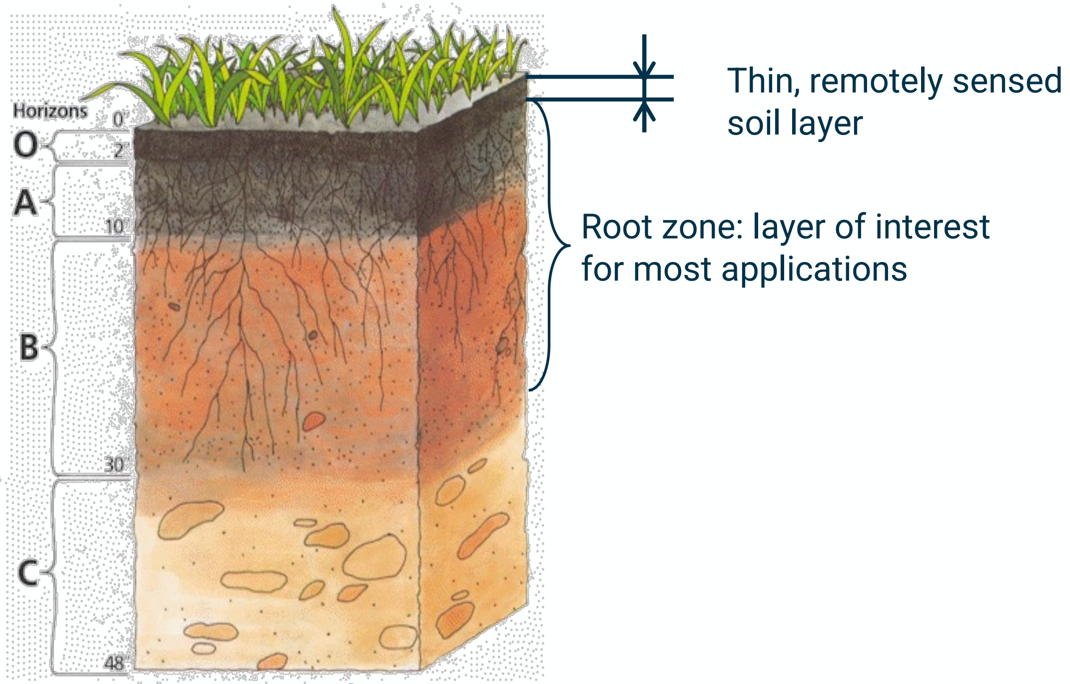

Soil profile

$$Mv = \frac{\text{Water Volume } (\mathrm{m}^3)}{\text{Total Volume } (\mathrm{m}^3)}$$

$$Mg = \frac{\text{Mass of water}}{\text{Mass of dry soil}}$$

https://www.geoengineer.org/education/soil-mechanics/soil-as-a-three-phase-system
https://www.nrcs.usda.gov/resources/education-and-teaching-materials/a-soil-profile

Context of Croplands

Soil moisture influences

Crop growth dynamics

Yield/production

Global food security

Field scale

Global scale

Soil moisture from SAR

Soil moisture retrieval from radar data: Ulaby,1974

Backscattering coefficient (σ°) = f (radar characteristics, target properties, etc).

Radar signals are more sensitive to soil moisture at low frequencies

High spatial resolution with SAR

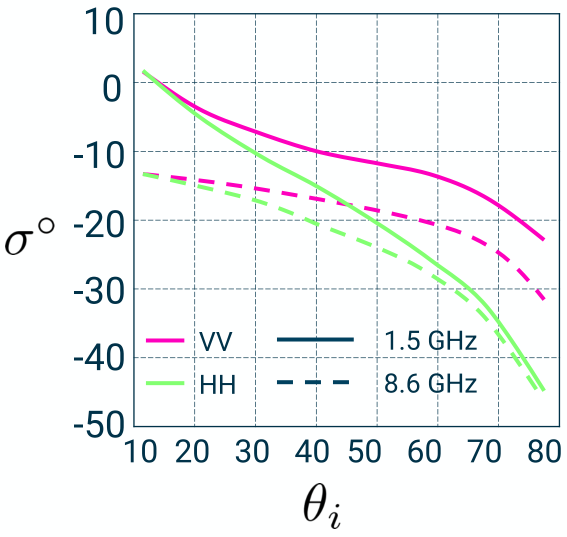

Radar backscatter intensity from a bare surface at various incidence angles (θ_i)

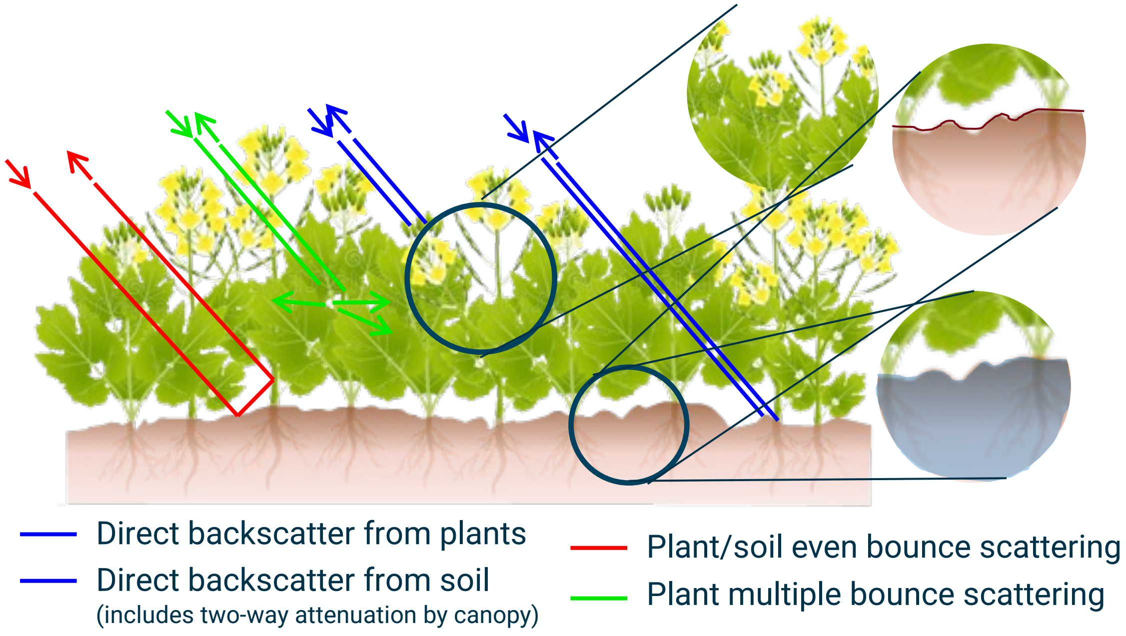

Scattering through vegetation canopy

Ulaby, F., 1974. Radar measurement of soil moisture content. IEEE Transactions on Antennas and propagation 22 (2), 257–265.
Fung, A.K., Chen, K.S. and Chen, K.S., 2010. *Microwave scattering and emission models for users*. Artech house.

Solving for volume scattering component

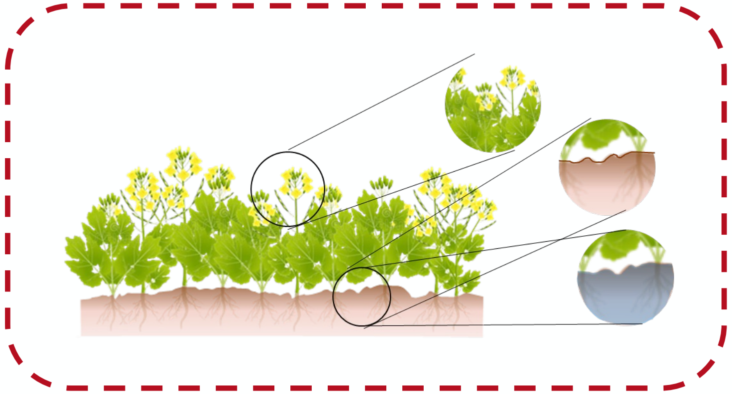

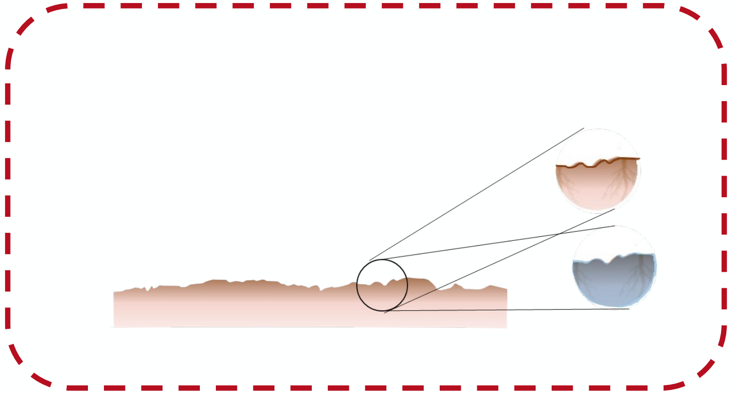

$$\mathbf{T}_3 = P_S\mathbf{T}_S + P_D\mathbf{T}_D + P_V\mathbf{T}_V$$

$$\mathbf{T}_3 - P_V\mathbf{T}_V = P_S\mathbf{T}_S + P_D\mathbf{T}_D$$

$$\det(\mathbf{T}_3 - P_V\mathbf{T}_V) = 0$$

or

$$\{\lambda_1, \lambda_2, \lambda_3\} = \mathrm{GEV}(\mathbf{T}_3, \mathbf{T}_V)$$

$$\Downarrow$$

$$P_V = \lambda_{min}$$

$$\mathbf{T}' = \mathbf{T}_3 - \lambda_{min}\mathbf{T}_V$$

1) $\mathbf{T}_V$ is a known positive-definite Hermitian matrix,
2) $\mathbf{T}_S$ and $\mathbf{T}_D$ are two unknown rank-1 matrices and
3) P_S, P_D, and P_V are unknown nonnegative expansion coefficients.

$$\mathrm{P}_r = 10\log_{10}(S_{\mathrm{VV}}S^*_{\mathrm{VV}}/S_{\mathrm{HH}}S^*_{\mathrm{HH}})$$

-2 dB > P_r	-2 dB < P_r < 2 dB	P_r > 2 dB
$[\mathbf{T}_V]_V = \frac{1}{30}\begin{bmatrix}15 & 5 & 0\\ 5 & 7 & 0\\ 0 & 0 & 8\end{bmatrix}$	$[\mathbf{T}_V]_R = \frac{1}{4}\begin{bmatrix}2 & 0 & 0\\ 0 & 1 & 0\\ 0 & 0 & 1\end{bmatrix}$	$[\mathbf{T}_V]_H = \frac{1}{30}\begin{bmatrix}15 & -5 & 0\\ -5 & 7 & 0\\ 0 & 0 & 8\end{bmatrix}$

Cui, Y., Yamaguchi, Y., Yang, J., Kobayashi, H., Park, S.-E., Singh, G., 2013. On complete model-based decomposition of polarimetric SAR coherency matrix data . IEEE transactions on geoscience and remote sensing 52 (4), 1991–2001.
Yamaguchi, Y., Moriyama, T., Ishido, M., Yamada, H., 2005. Four-component scattering model for polarimetric SAR image decomposition. IEEE Transactions on geoscience and remote sensing 43 (8), 1699–1706.

Extracting and modelling the surface scattering

$$\mathbf{T}' = \mathbf{T}_3 - \lambda_{min}\mathbf{T}_V$$

$$\Downarrow$$

$$\mathbf{T}' = \lambda_1 \mathbf{k}_1 \mathbf{k}_1^{*\mathrm{T}} + \lambda_2 \mathbf{k}_2 \mathbf{k}_2^{*\mathrm{T}}$$

where, $\lambda_1 \geq \lambda_2$

$\mathbf{T}'$ is positive semidefinite with rank-2
$\mathbf{T}'$ contains upto two single scatterers
$\mathbf{T}'$ can be written as sum of two rank-1 matrices

X-Bragg model

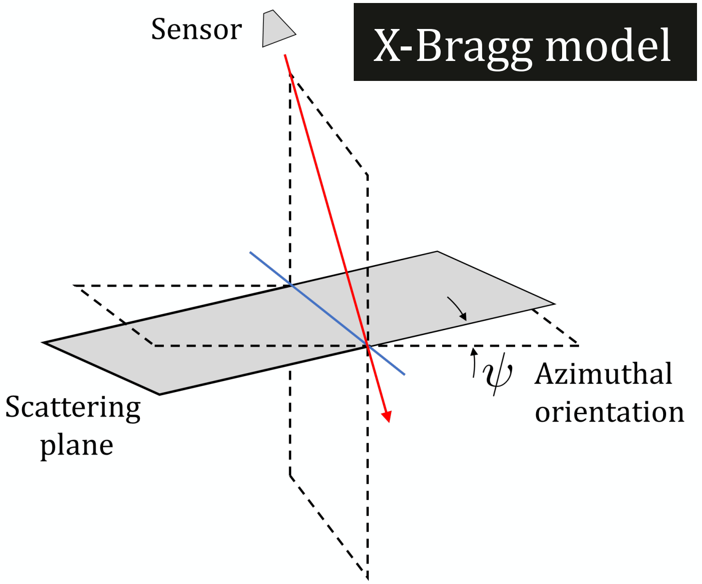

$$\mathbf{T}_{\mathrm{XB}} = f_s \begin{bmatrix} 1 & \beta^* \operatorname{sinc}(2\psi) & 0 \\ \beta \operatorname{sinc}(2\psi) & \frac{1}{2}|\beta|^2 (1 + \operatorname{sinc}(4\psi)) & 0 \\ 0 & 0 & \frac{1}{2}|\beta|^2 (1 - \operatorname{sinc}(4\psi)) \end{bmatrix}$$

here, f_s and β are surface scattering intensity and surface scattering mechanism ratio respectively and are defined as,

$$\beta = \frac{R_\parallel - R_\perp}{R_\parallel + R_\perp} \quad \text{and} \quad f_s = \frac{m_s^2}{2}|R_\parallel + R_\perp|^2$$

$$R_\parallel = \frac{\cos\phi_i - \sqrt{\varepsilon_r - \sin^2\phi_i}}{\cos\phi_i + \sqrt{\varepsilon_r - \sin^2\phi_i}}$$

$$R_\perp = \frac{(\varepsilon_r - 1)(\sin^2\phi_i - \varepsilon_r(1 + \sin^2\phi_i))}{(\varepsilon_r \cos\phi_i + \sqrt{\varepsilon_r - \sin^2\phi_i})^2}$$

ϕ_i-incidence angle
ε_r-soil permittivity
ψ-azimuthal orientation

Hajnsek, I., 2001. Inversion of surface parameters using polarimetric SAR. PhD Thesis.

Sensitivity of θ_{FP} and $\overline{\alpha}$ towards soil dielectric and roughness

$$\overline{\alpha}_{\mathrm{XB}} = \frac{\lambda_{1_{\mathrm{XB}}}\alpha_{1_{\mathrm{XB}}} + \lambda_{2_{\mathrm{XB}}}\alpha_{2_{\mathrm{XB}}} + \lambda_{3_{\mathrm{XB}}}\alpha_{3_{\mathrm{XB}}}}{\lambda_{1_{\mathrm{XB}}} + \lambda_{2_{\mathrm{XB}}} + \lambda_{3_{\mathrm{XB}}}}$$

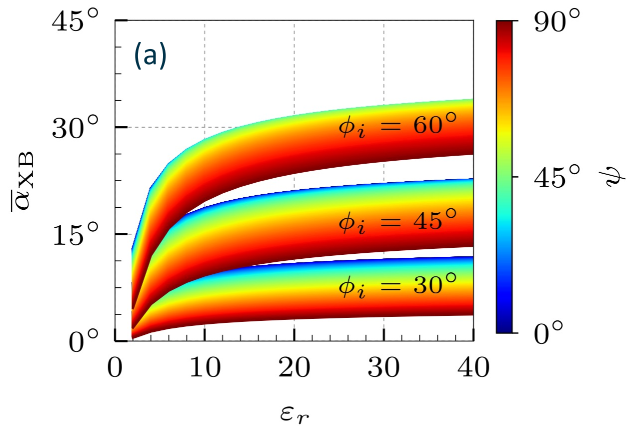

$$\theta_{\mathrm{FP}_{\mathrm{XB}}} = \tan^{-1}\left(\frac{m_{\mathrm{XB}}\,\mathrm{Span}\,(T_{11} - T_{22} - T_{33})}{T_{11}\,(T_{22} + T_{33}) + m_{\mathrm{XB}}^2\,\mathrm{Span}^2}\right)$$

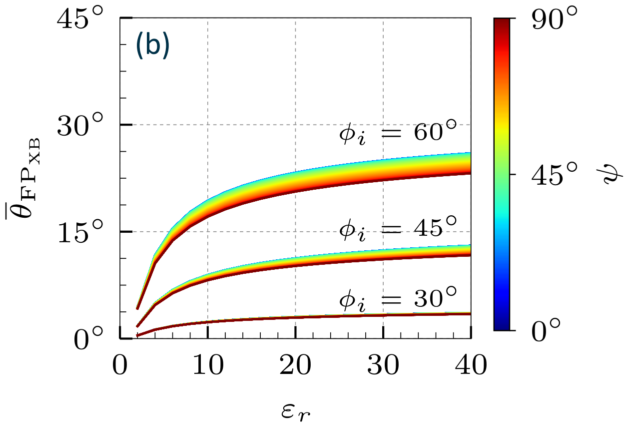

(a) $\overline{\alpha}_{\mathrm{XB}}$ and (b) $\overline{\theta}_{\mathrm{FP}_{\mathrm{XB}}} = 45° - \theta_{\mathrm{FP}_{\mathrm{XB}}}$ as a function of the soil permittivity ε_r and surface roughness ψ at different local incidence angles ϕ_i.

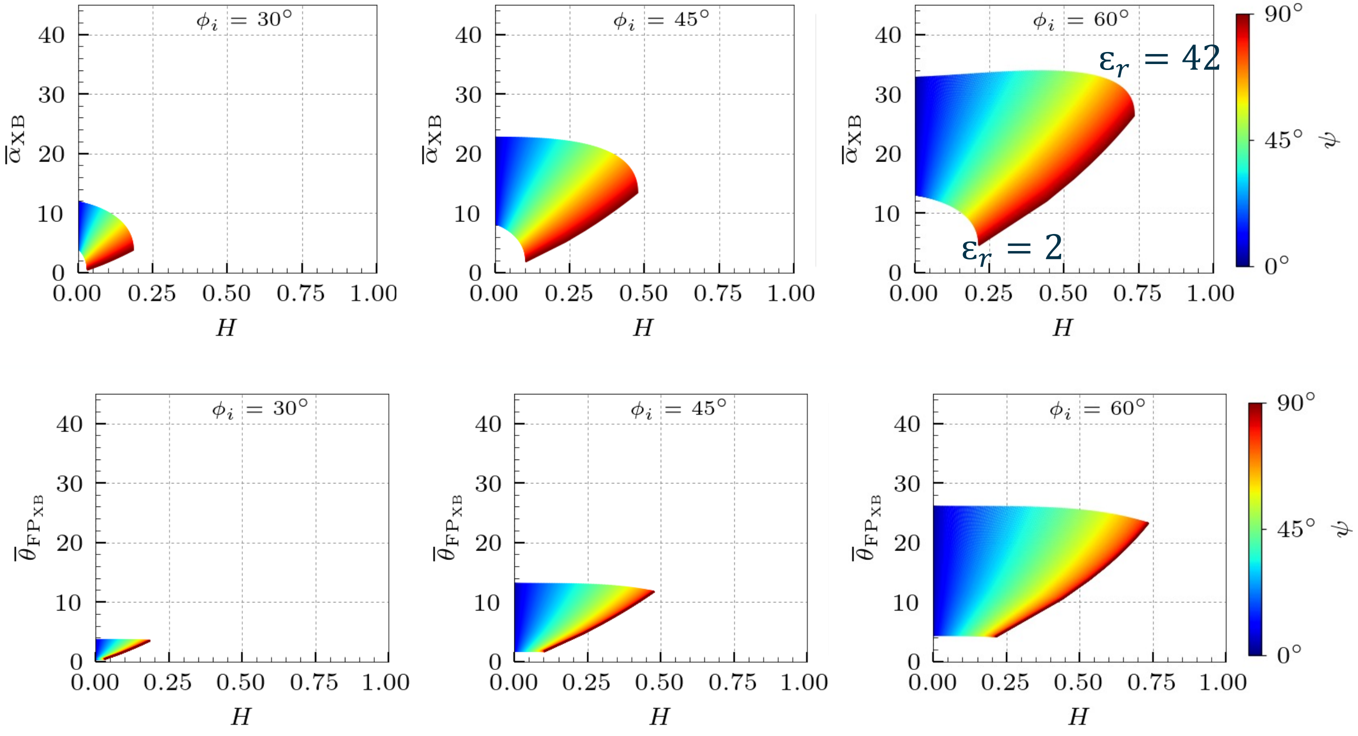

Simulation plots of $H - \bar{\alpha}_{\mathrm{XB}}$ and $H - \bar{\theta}_{\mathrm{FP}_{\mathrm{XB}}}$ as a function of the soil permittivity ε_r, and surface roughness ψ at different local incidence angles ϕ_i.

Cloude, S. R., 2009. Polarisation: Applications in Remote Sensing. Oxford University Press.
Dey, S., Bhattacharya, A., Ratha, D., Mandal, D., Frery, A. C., 2020. Target Characterization and Scattering Power Decomposition for Full and Compact Polarimetric SAR Data . IEEE Transactions on Geoscience and Remote Sensing 59 (5), 3981–3998.

Methodology

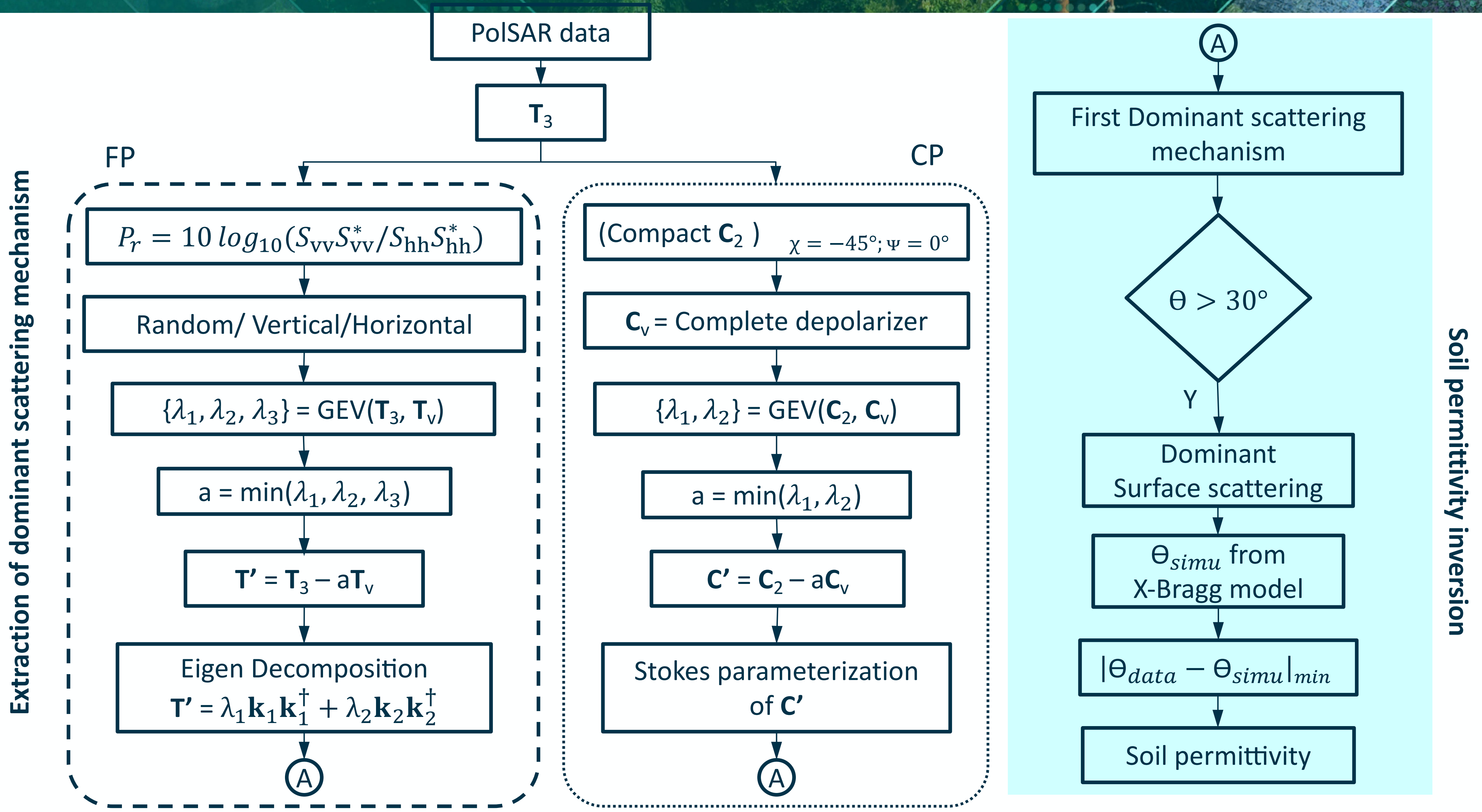

Bhogapurapu, N., Dey, S., Bhattacharya, A., López-Martínez, C., Hajnsek, I., & Rao, Y. S. (2022). Soil Permittivity Estimation Over Croplands Using Full and Compact Polarimetric SAR Data. *IEEE Transactions on Geoscience and Remote Sensing*, *60*, 1-17.

Study area & dataset

Test site: Soil Moisture Active Passive Validation Experiment 2012 (SMAPVEX12) test site located in Manitoba, Canada.

Crops: Canola, Corn, Pasture, Soybean

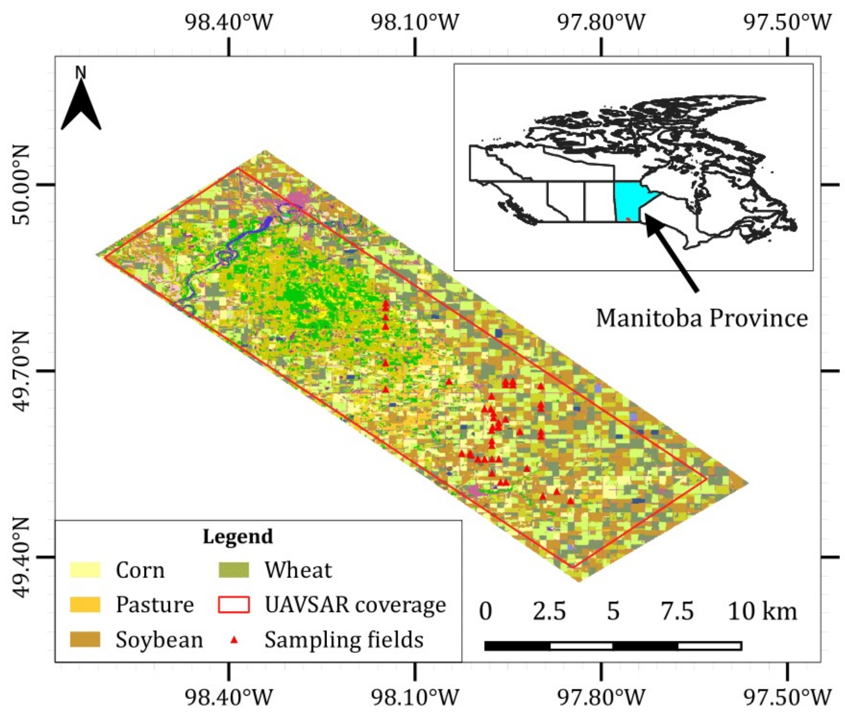

Manitoba, Canada

Table 1: Specifications of UAVSAR data (Full-pol/MLC GRD) used in this study (flight line ID: #31606) along with corresponding dates of in-situ measurements.

Day of Year (DOY)	Date of SAR data acquisition	Flight ID	Range of incidence angle (Deg.)	Date of In-situ measurements
169	6/17/2012	12044	22.59-65.18	6/17/2012
174	6/23/2012	12046	22.73-66.32	6/23/2012
175	6/24/2012	12047	21.32-65.42	6/24/2012
177	6/25/2012	12048	21.38-66.68	6/25/2012
179	6/27/2012	12049	22.83-67.42	6/27/2012
181	6/29/2012	12050	21.31-65.52	6/29/2012
185	7/03/2012	12055	21.34-66.14	7/08/2012
187	7/05/2012	12056	22.56-65.83	7/05/2012
192	7/10/2012	12058	22.54-66.16	7/10/2012
195	7/13/2012	12059	22.54-66.16	7/13/2012
196	7/14/2012	12060	22.54-66.16	7/14/2012
199	7/17/2012	12061	21.45-66.52	7/17/2012

Entropy-Alpha analysis

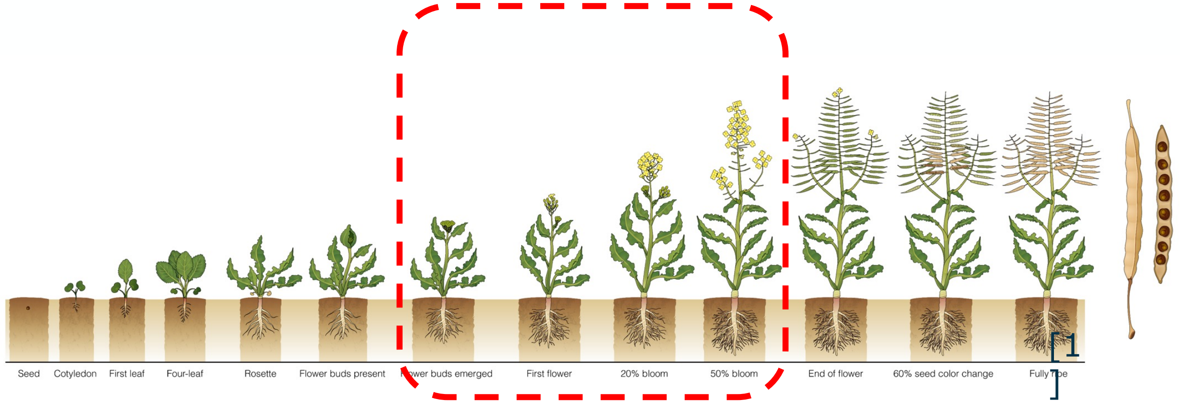

Phenology stages of canola from sowing to maturity. phenooy stages corresponds to the data utilised in this study are also highlighted

- During DOY-168 DOY-199: inflorescence emergence and flowering & pod development
- Observed H= 0.73 ± 0.06, $\bar{\alpha}$ = 39.98 ± 4.19
- Majority of the sampling points are in transition between Zone-6 and Zone-5
- Zone-5: medium entropy vegetation scattering
- Zone-6: medium entropy surface scatterer
- Residual H = 0.50 ± 0.06, $\bar{\alpha}$ = 36.88 ± 4.87
- Zone-9 : low entropy surface scatterer

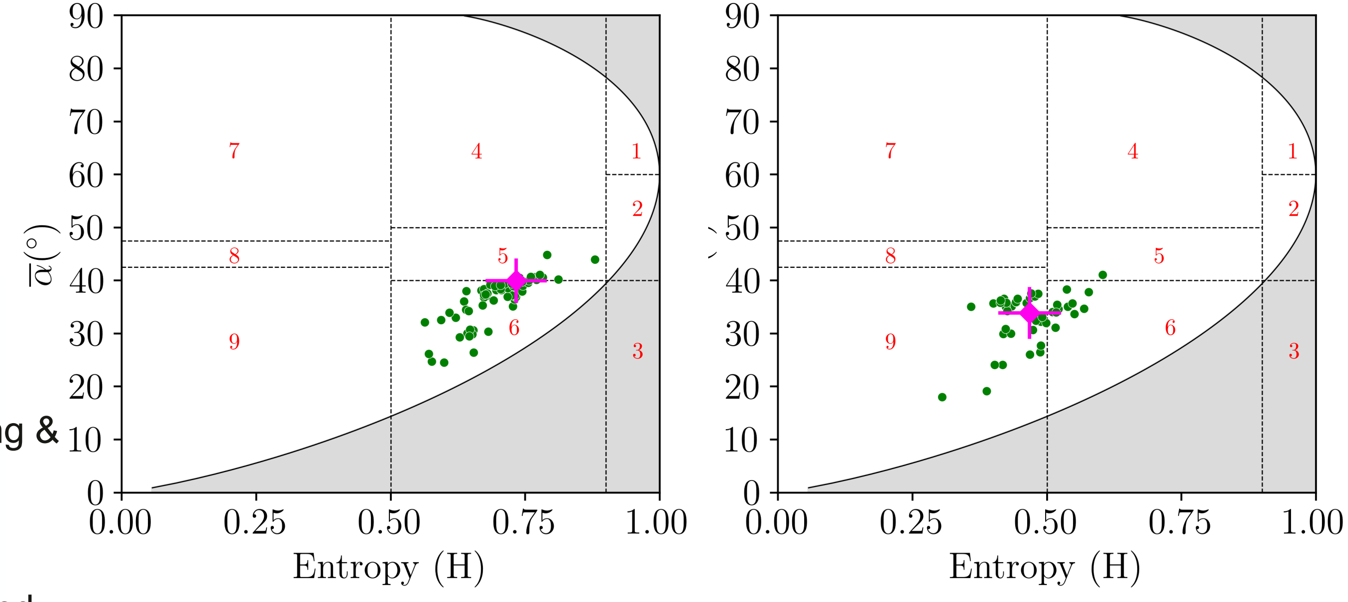

(a) (b)

PolSAR data distribution of canola (a) from observed coherency matrix $\mathbf{T}$ (b) after deducting the volume scattering contribution ($\mathbf{T} - P_V\mathbf{T}_V$). The cluster mean along with standard deviation is shown in magenta.

Results over canola

- With $\bar{\alpha}$: RMSE of 9.92 and r = 0.77
- With θ_{FP} : RMSE of 5.90 and r = 0.83
- Over estimation with $\bar{\alpha}$ → effect of depolarization term
- Temporal dynamics of the estimated and observed soil permittivity are good agreement
- we observe a marginal increase in uncertainty of estimates from DOY-181
- Due to an increase in complexity of the canopy during the pod initiation stage

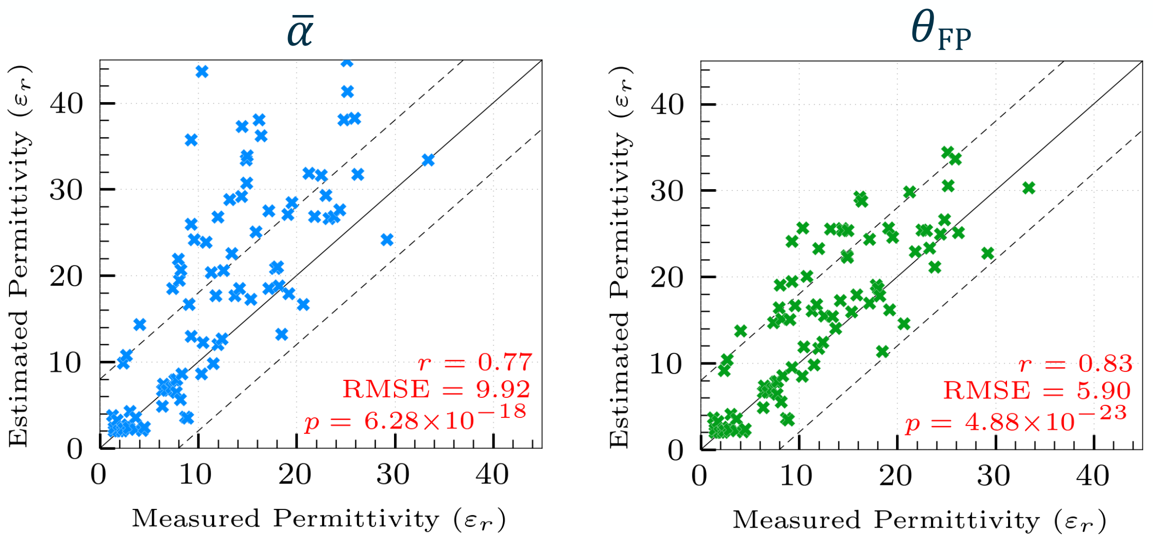

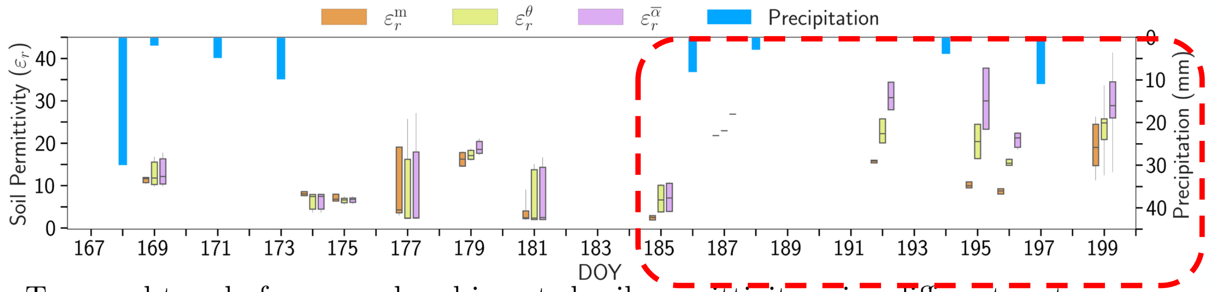

Temporal trend of measured and inverted soil permittivity using different scattering mechanisms.

Bhogapurapu, N., Dey, S., Bhattacharya, A., López-Martínez, C., Hajnsek, I., & Rao, Y. S. (2022, July). Soil permittivity estimation over croplands using PolSAR data. In *IGARSS 2022-2022 IEEE International Geoscience and Remote Sensing Symposium* (pp. 8000-8003). IEEE.

Converting permittivity to Soil moisture

Soil permittivity → volumetric soil moisture.

- Theoretical mixing model
- Mixing models combined with phenomenological material equations
- Empirical mixing models

$$m_v = -5.3 * 10^{-2} + 2.92 * 10^{-2}\varepsilon_r - 5.5 * 10^{-4}\varepsilon_r^2 + 4.3 * 10^{-6}\varepsilon_r^3$$

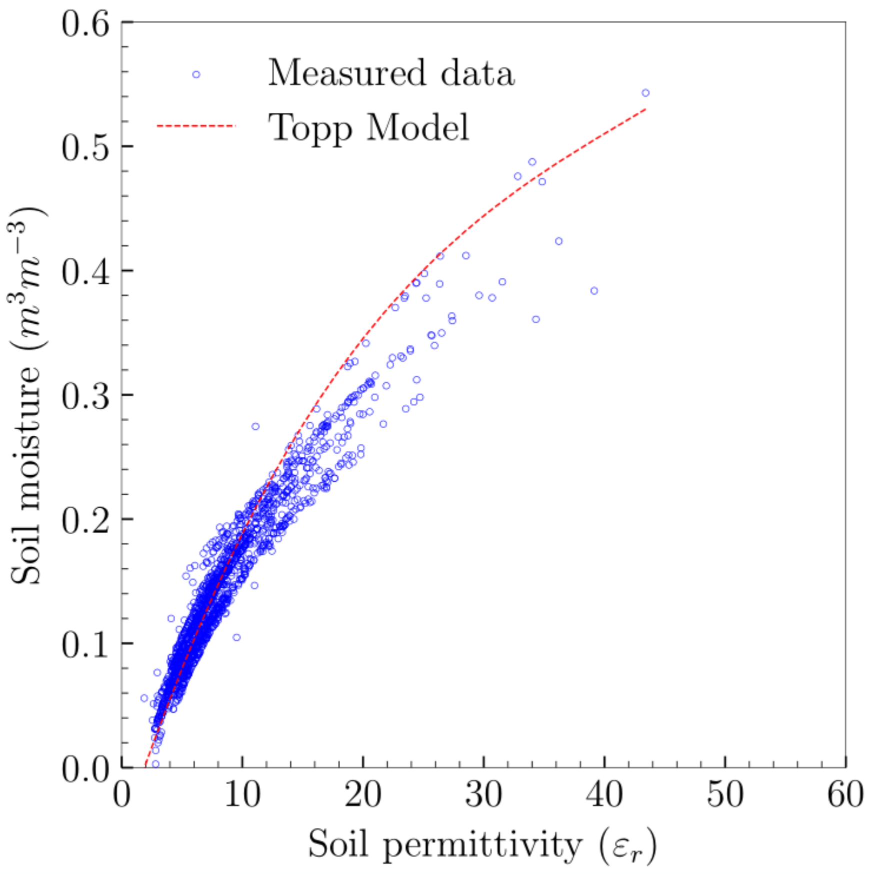

Correlation plot of field measured soil permittivity and soil moisture. Topp's model output also plotted for comparison purpose.

Topp, G. C., Davis, J. L., & Annan, A. P. (1980). Electromagnetic determination of soil water content: Measurements in coaxial transmission lines. *Water resources research*, *16*(3), 574-582.

Surface scattering models for soil permittivity

Dubois et al. (1995)

$$\sigma^{\circ}_{\mathrm{hh}} = 10^{-2.75}\frac{\cos^{1.5}\theta}{\sin^5\theta}\;10^{0.028\varepsilon'\tan\theta}(ks\sin\theta)^{1.4}\lambda^{0.7}$$

$$\sigma^{\circ}_{\mathrm{vv}} = 10^{-2.37}\frac{\cos^{3}\theta}{\sin^3\theta}\;10^{0.046\varepsilon'\tan\theta}(ks\sin\theta)^{1.1}\lambda^{0.7}$$

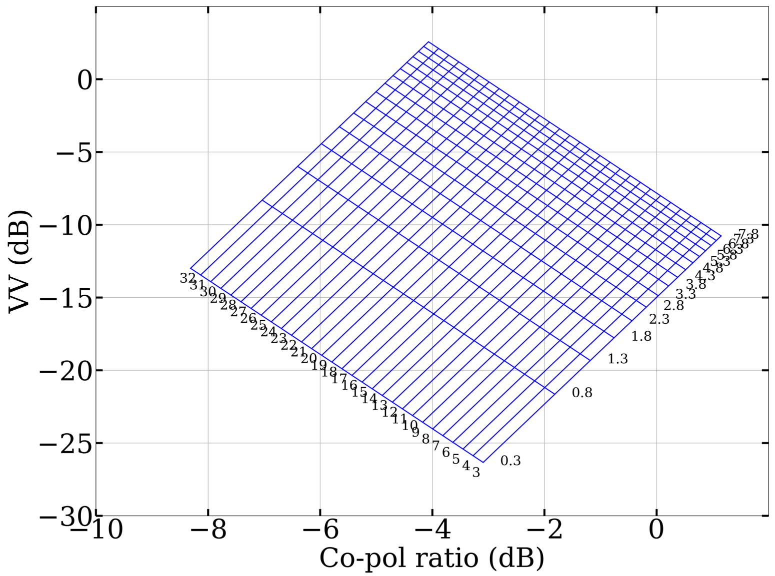

Oh (2004)

$$\frac{\sigma^{\circ}_{hh}}{\sigma^{\circ}_{vv}} = 1 - \left(\frac{2\theta}{\pi}\right)^{0.35 m_v^{-0.65}} e^{-0.4(ks)^{1.4}}$$

$$\frac{\sigma^{\circ}_{vh}}{\sigma^{\circ}_{vv}} = 0.095(0.13 + \sin 1.5\theta)^{1.4}(1 - e^{1.3(ks)^{0.9}})$$

$$\sigma^{\circ}_{hv} = 0.11 m_v^{0.7}\cos^{2.2}\theta(1 - e^{-0.32ks^{1.8}})$$

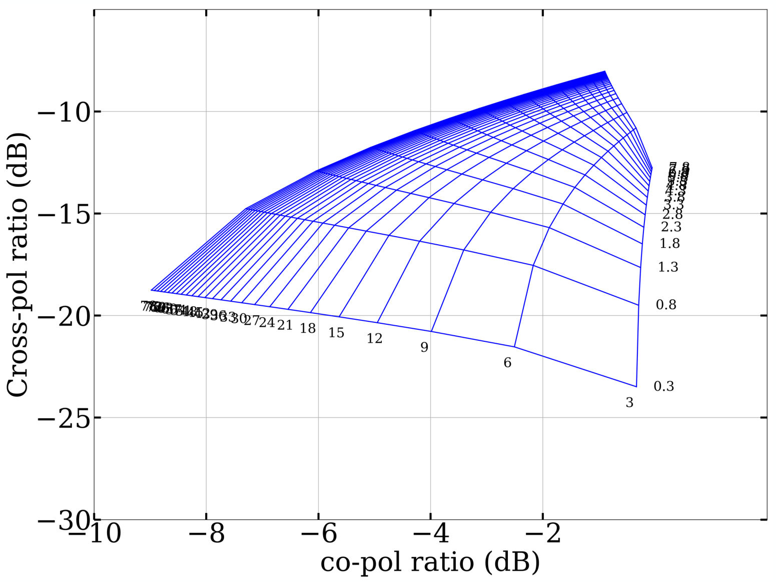

Yisok Oh, "Quantitative retrieval of soil moisture content and surface roughness from multipolarized radar observations of bare soil surfaces," in *IEEE Transactions on Geoscience and Remote Sensing*, vol. 42, no. 3, pp. 596-601, March 2004, doi: 10.1109/TGRS.2003.821065.
Dubois, Pascale C and Van Zyl, Jakob and Engman, Ted, "Measuring soil moisture with imaging radars," IEEE transactions on geoscience and remote sensing, vol. 33, pp. 915--926, 1995.

Permittivity estimates with various models

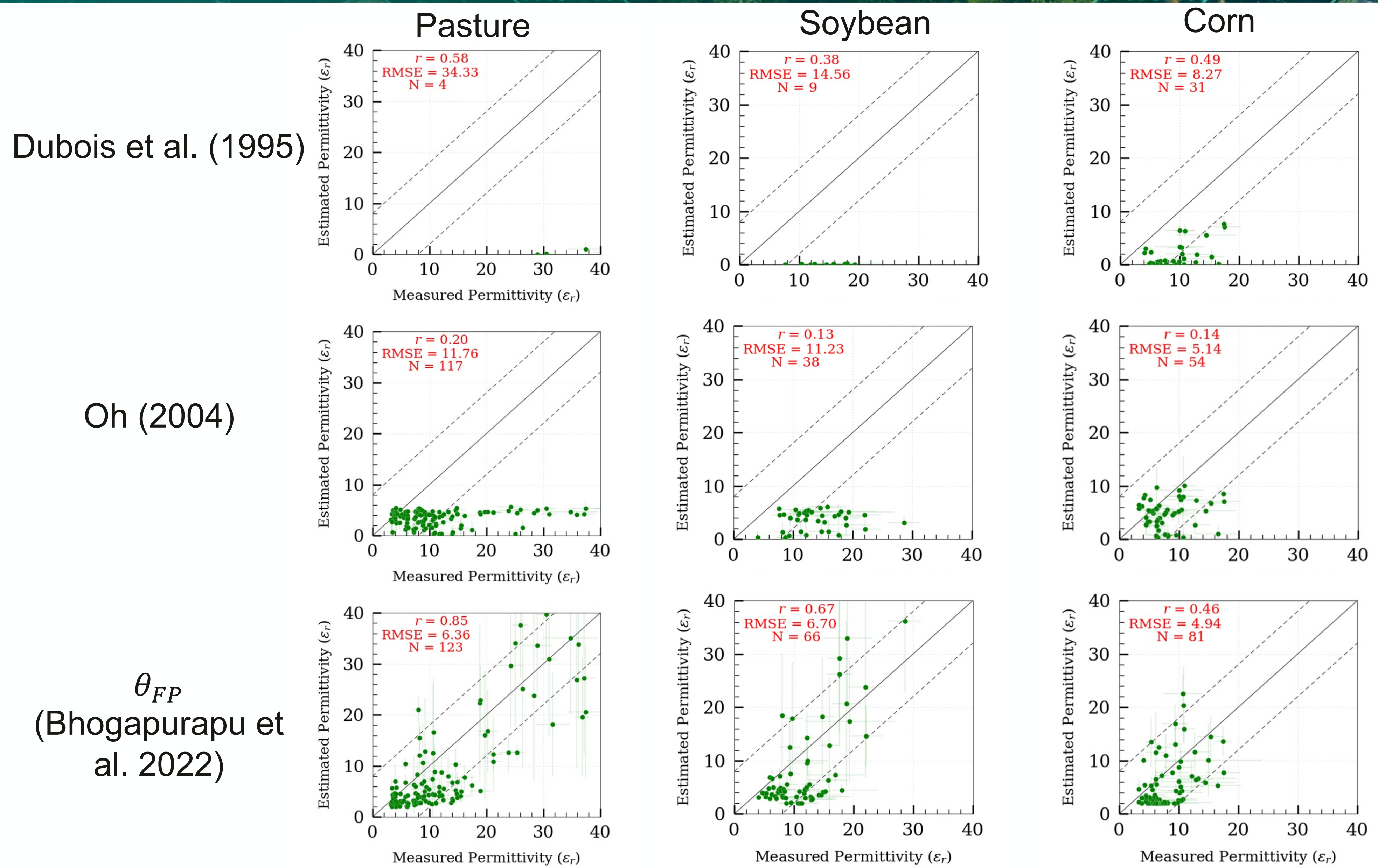

Temporal permittivity maps

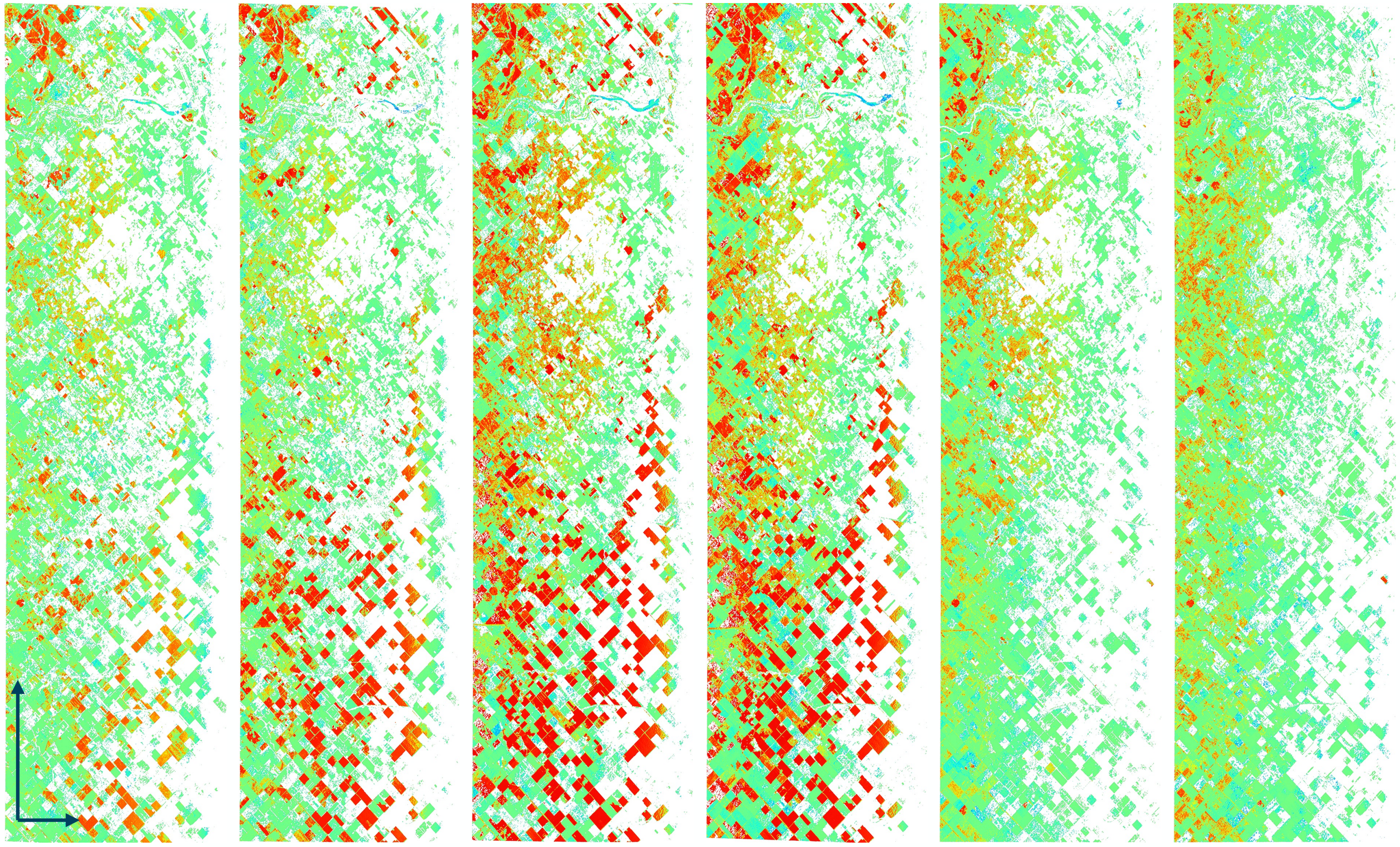

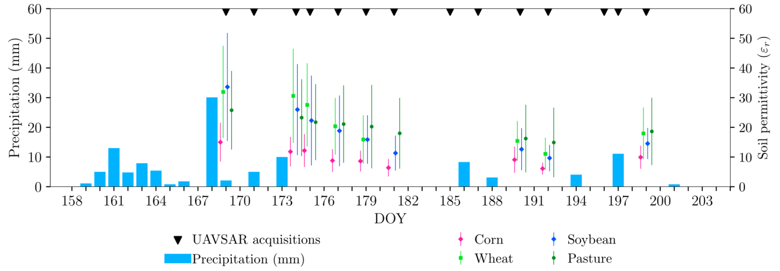

Spatiotemporal maps of the estimated soil permittivity

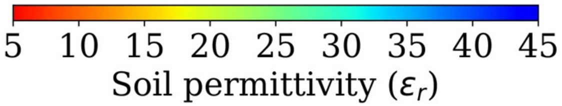

Summary

- Presented a methodology for soil permittivity estimation over croplands.
- Evaluated the performance of the proposed technique to estimate soil permittivity over four crops→ major phenology stages.
- With θ_{FP} we obtain Root Mean Square Error of 4.9 – 6.7.
- Qualitative analysis of spatio-temporal soil permittivity maps are in very good agreement with in-situ data.

Advantages:

- ✓ Minimum effect of surface roughness
- ✓ 1-D minimization
- ✓ Generalized framework for full- and compact-pol SAR configuration

- Further, a comprehensive comparative analysis is required with various decomposition techniques.
- Extended Fresnel Scattering Model regarding the depolarization of dihedral-type scattering.

Thank you!

Questions?